

Copyright © [2006] IEEE. Reprinted from

(Special Issue on Nonlocal, Collisionless Electron Transport in Plasmas - June 2006) .

This material is posted here with permission of the IEEE. Internal or personal use of this material is permitted. However, permission to reprint/republish this material for advertising or promotional purposes or for creating new collective works for resale or redistribution must be obtained from the IEEE by writing to pubs-permissions@ieee.org.

By choosing to view this document, you agree to all provisions of the copyright laws protecting it.

Experimental and Theoretical Study of RF Plasma at Low and High Frequency.

T.V. Rakhimova, O.V. Braginsky, V.V. Ivanov, T.K. Kim, J.T. Kong, A.S. Kovalev, D.V. Lopaev, Yu.A. Mankelevich, O.V. Proshina, A.N. Vasilieva.

Abstract--A capacitive coupled radio-frequency plasma at argon pressure of 100 mTorr, 13.56 and 81 MHz frequency and high specific input powers has been studied both experimentally and theoretically. The different numerical models were developed and used for simulation. It was shown that the main ionization source in low frequency (LF) discharge at all studied powers is due to secondary electrons emitted from the electrode by ion impact. The high frequency (HF) discharge at the same powers is operated in α -mode. Applicability of fluid and kinetic models for simulation of LF and HF discharges are studied on the base of our experimental data.

Index Terms--capacitive coupled radio-frequency plasma, high specific power, low (LF) and high frequency (HF) plasma, particle-in-cell (PIC) simulation

I. INTRODUCTION

Last time both fluid [1] and PIC [2-4] models of double frequency (DF) discharges have been developed. It is important to note that the plasma processing in DF reactors are carried out at specific input power more than $P > 0.5$ W/cm². At these power conditions the influence of secondary electron emission (γ -electrons) and gas heating on discharge self-organization should be studied. For this goal a comprehensive experimental and theoretical study of single frequency discharge at high power is needed.

In [3-4], the simulation of both single (SF) and dual frequencies discharges was carried out. Unfortunately, the absence of comparison of simulation results with experimental data does not allow to study discharge structure at high specific power in details.

Single frequency and double frequency discharges were studied both experimentally and theoretically in wide range of specific input powers. Vast volume of information obtained from probe and emission spectroscopy measurements does not come within the province of this paper and will be described in

T.K. Kim and J.T. Kong are with CAE, Semiconductor R&D center, Samsung Electronics, Republic of Korea, E-mail: taikyung.kim@samsung.com

detail in future publications. In this paper, the emphasis is on the peculiarities of the discharges on low (LF) and high (HF) frequencies for high specific power inputs.

One of the important problems in the study of such discharges is the possibility to use more simple and fast model to reduce huge computational times. Huge computational time is required even for fast PIC MC models of the reactor processes in complex multi-component gas mixtures. It should be noted that the use of analytical or semi-analytical approaches seems to be very attractive but deal with additional problems: dividing electrons on different groups ("fast", "middle", "slow"), setting charge fluxes on the boundaries of electrode sheathes and so on. This is make such approaches more methodical rather than practical and allows to study qualitatively the problems.

So the purpose of this paper is to study the possibility to use modifications of fluid models and to compare the calculated results with PIC MC model calculations and experimental results, and to reveal non-adequate features of such fast models in simulations of rf discharges. To simplify the rf discharge simulations the experiments were carried out in the specially designed symmetric reactor.

Following one-dimensional models were developed and used:

1. PIC MC hybrid model (PIC MC for electron motion, fluid for ion concentrations with momentum transfer equation for ions fluxes).
2. Fluid model for electrons and ions.

All results in this paper are presented for argon of 100 mTorr pressure. Low frequency is 13.56 and high frequency is 81 MHz.

II. EXPERIMENTAL SET-UP.

A schematic diagram of the discharge chamber is shown in Figure 1. The inner diameter of the quartz discharge tube is 100 mm. The distance between two electrodes is 24 mm and the diameter of the electrodes is 80 mm. The top electrode can be water-cooled. Gas inlet is mounted in the top electrode, and the exhaust was led out through the bottom electrode. The bottom electrode was grounded, and the RF power from one (Single frequency, SF) or two (Dual frequency, DF) generators was transferred to the top electrode. In DF plasma

Manuscript received August 3, 2005. This work was supported by Samsung-MSU Contract, RFBR-05-02-17649 and Russian Federal Science-Technology Program 02.445.11.7201.

T.V. Rakhimova, O.V. Braginsky, V.V. Ivanov, A.S. Kovalev, D.V. Lopaev, Yu.A. Mankelevich, O.V. Proshina, A.N. Vasilieva are with Skobeltsyn Institute of Nuclear Physics, Lomonosov Moscow State University, Vorob'evy Gory, Moscow 119992, Russia (Phone: +7-495-9394957, E-mail: TRakhimova@mics.msu.su)

low frequency (LF) was 13.56MHz (or 1.76 MHz) and high

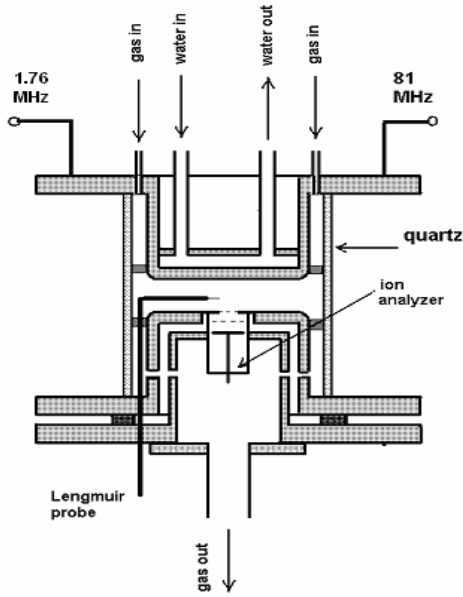


Fig. 1. Schematic diagram of the discharge chamber.

frequency (HF) was 81.36 MHz. Powers of both generators were up to 250 W. The RF generators were coupled to the top electrode by using the matching networks and RF filters. The RF powers dissipated in the discharge at every of frequencies were measured by power-meters of forward and reflected waves. The voltages on both frequencies applied to the top electrode were measured by two voltmeters with RF resonance filters.

Plasma parameters were measured by using the Langmuir probe technique. The plasma density and electron temperature were deduced from ion saturation current and I-V characteristics slope respectively. A Langmuir probe tip was 300 μm in diameter and 3 mm length. The probe could be moved along the axis between electrodes and along radius of the discharge chamber. Thus, distributions of plasma density and electron temperature were measured both between electrodes and on radius of the discharge chamber.

III. NUMERICAL MODELS.

A. PIC MC Hybrid model (Model 1).

In order to describe accurately the electron motion, a PIC-MC method is used [5]. This method consists of integrating the equations of motion for a number of super-electrons. Every super-electron is composed of a large number of real electrons, moving with the same velocity. In the 1D model, the equations of motion take the form

$$m \frac{d^2 z}{dt^2} = eE(z, t), \quad m \frac{d^2 x}{dt^2} = 0, \quad m \frac{d^2 y}{dt^2} = 0. \quad (1)$$

To solve the equations, a second order finite-difference scheme was used. The electron density n_e , which is used

later in solving the Poisson equation, is determined by linear interpolation according to the new locations of the super-electrons and the super-electron weights. The electron wall reflection ratio is set equal to zero, i.e., each super-electron is removed from the model when it reaches the walls.

During each time step, every super-electron may participate in electron-electron or one of the electron-neutral processes given in Table I. The probabilities of the processes are evaluated by the formula

$$W = Nv\sigma dt, \quad (2)$$

where N is the density of the target species, v is the electron velocity, σ is the cross section of the processes, and dt is the time step. The energy loss of electrons with energy ϵ and mass m due to elastic collisions with molecules of mass M is calculated by $\Delta \epsilon = \epsilon \cdot 2m/M$. The electron energy loss due to inelastic collisions was equal to the excitation energy or ionization potential. The sum of the energy of the primary and secondary electrons, which are formed after ionization, is equal to the difference between the initial energy of the primary electron and the ionization energy. The total energy is divided in a random way between these two electrons. The experimental momentum cross sections were used for elastic collisions to describe correctly the electron drift velocity. Electron-electron collisions with energy of second electron smaller than first one were considered to eliminate double calculation of e-e collision. E-e cross-section was chosen as a function of high energy (first) electron only, which permits to decrease computation time.

The choice of the time step is predominantly determined by two factors. First, it is related to the simulation of the elementary processes, i.e. an electron can at maximum participate in only one process per time step. Consequently, the time step must be much less than the characteristic time of the process having the largest cross section. Second, it is governed by the errors appearing when the equations of motion for electrons moving in the spatially non-uniform field are numerically integrated. This restriction can be estimated by using the following expression [6]:

$$dt \ll \sqrt{\frac{\langle \epsilon \rangle D_i}{eL^2 \langle v \rangle^3 \left(\frac{\partial^2 E}{\partial z^2} \right)_{\max}}} \quad (3)$$

Here, $\langle \epsilon \rangle$ is the average electron energy, $\langle v \rangle$ is the average electron velocity, L is the characteristic dimension of the plasma, and D_i is the ion diffusion coefficient. This expression guarantees a good accuracy of the integration of the electron motion equation for the characteristic time of an electron life in the discharge, which is determined by ion diffusion.

It is clear that the superparticle weight determines the accuracy and the calculation time, i.e., a large superparticle weight (corresponding to a small number of superparticles) results in poor statistics and hence poor accuracy, whereas a small superparticle weight (corresponding to a large number of superparticles) results in better accuracy but a long

calculation time. We used 32000-64000 superelectrons in our calculations.

The number of these superelectrons was modified in the algorithm due to ionization processes and loss of superelectrons at the wall. To keep the overall number of superelectrons approximately constant we modified their weight and number. If the overall number of the superelectrons exceeded 110% of the required value, then 1% of occasionally chosen superelectrons were "killed," whereas the size of other superelectrons was increased by 1% to keep the overall charge of superelectrons unchanged. If the overall number of the superelectrons reduced to 90% of the required value, then 1% of the occasionally chosen superelectrons were doubled, whereas the size of all superelectrons was decreased by 1%. Superelectron weight modification was carried out at a fixed phase of rf discharge. It prevents unwanted switching of this mechanism due to changing of the super-electron number with rf phase.

To reduce the simulation time we used hydrodynamic approach for ions motion.

Spatial distributions of ions are calculated from continuity equations:

$$\frac{\partial n_i(z, t)}{\partial t} = -\frac{\partial \Gamma_i}{\partial z} + S_i(z, t) \quad (4)$$

$$\Gamma_i = v_i n_i - D_i \nabla n_i$$

where n_i – concentration of i -type ions (Ar^+ for the experiments in Ar), v_i is the drift velocity. The ion fluxes are calculated by modeling the momentum transfer equation:

$$M_i n_i \left(\frac{\partial v_i}{\partial t} + (v_i \nabla) v_i \right) = e_i n_i \bar{E} + R_i \quad (5)$$

$$R_i = \sum_j R_{ij} \quad (6)$$

$$R_{ij} = -n_i \mu_{ij} \frac{v_i - v_j}{\tau_{ij}} \quad (7)$$

where μ_{ij} and D_i – are the normalized mass and diffusion coefficients for i ions, E – electric field, τ_{ij} is characteristic time of scattering of i - ion on j particle (Ar^+ on Ar for example).

The source term S_i represents the creation and destruction of the particles by electron impact collisions (see Table 1). The cross sections of these processes were taken from [7].

As mentioned above, at each time step when the super-electrons are followed, the balance equations for the various ions and neutral species are also solved, together with Poisson's equation

$$\frac{\partial E}{\partial z} = 4\pi e(n_i - n_e). \quad (8)$$

The potential at the grounded electron is set equal to zero. The potential at the driven electrode is set equal to

TABLE I
ELECTRON-NEUTRAL COLLISIONS, USED IN THE MODEL

Type of collision	Reaction	Threshold (eV)	Ref.
Elastic scattering	$e + Ar \rightarrow e + Ar$		^{a)}
Excitation of metastable states (with cascade processes)	$e + Ar \rightarrow e + Ar^*$	11.55	^{a)}
Excitation of low resonance states (with cascade processes)	$e + Ar \rightarrow e + Ar^{**}$	11.62	^{a)}
Ionization	$e + Ar \rightarrow e + e + Ar^+$	15.75	^{a)}
Stepwise ionization	$e + Ar^* \rightarrow e + e + Ar^+$	4.2	[10]

^{a)} See the text

$$V_{(z=L)} = -\int_0^L E dz = V_{rf} \sin(2\pi v_{rf} t), \quad (9)$$

where V_{rf} and v_{rf} are the amplitude and the frequency of the applied potential, respectively. The value of V_{rf} is adjusted until the dissipated power in the discharge equals the experimental value of electric input power. No dc self-bias voltage is considered in this 1D model.

The boundary conditions for ions:

$$\Gamma_i \Big|_{z=0,L} = \gamma_{ion}^i n_i v_i \Big|_{z=0,L} \quad (10)$$

where γ_{ion}^i is the loss probability for i -type ions. At our experimental conditions the value of γ_{ion}^i for Ar^+ ions was equal 1.

Electrons are absorbed and ions are neutralized on the electrodes. Secondary electron emission from electrodes due to ion impacts is included.

Spatial distributions of all neutral species (including lowest metastable Ar^* and resonance Ar^{**} argon states) are calculated from continuity equations:

$$\frac{\partial n_k(z, t)}{\partial t} = -\frac{\partial \Gamma_k}{\partial z} + S_k(z, t) \quad (11)$$

where n_k is the concentration of k -type species, $\Gamma_k = -D_k \partial n_k / \partial z$ is the diffusion flux, D_k is diffusion coefficient, S_k is the total rate of creation and destruction of given species in different reactions (Table 1).

The boundary conditions for neutral species:

$$\Gamma_i \Big|_{z=0,L} = \gamma_i \frac{n_i v_{ti}}{4} \Big|_{z=0,L} \quad (12)$$

v_{ti} is the thermal velocity, γ_i is the loss probability for i -type species. In the model the loss probabilities for Ar^* and Ar^{**} are equal 1. The total pressure p_{tot} in the model is given by the ideal gas law

$$p_{tot} = k_b T_g \sum n_i, \quad (13)$$

where k_b is the Boltzmann constant and T_g is the gas temperature.

The spatial distribution of gas temperature $T_g(z,t)$ is calculated from the equation:

$$\frac{\partial T_g(z,t)}{\partial t} + \frac{1}{c_p N} \frac{\partial Q}{\partial z} = \frac{1}{c_p N} S_Q(z,t) \quad (14)$$

where $Q = -\lambda \frac{\partial T}{\partial z}$ is the heat flux density, λ is the heat

conductivity coefficient, c_p is the heat capacity per one molecule. S_Q is the total density of heat sources and heat losses caused by different chemical reactions.

The boundary condition for equation (14):

$$T_g|_{z=0,L} = T_0 \quad (15)$$

where T_0 is the electrode temperature. At our experimental conditions T_0 is equal 300 K. Gas temperature was not measured experimentally.

In this model known numerical method of speeding up the PIC calculation (longer ion time steps) is applied. One of "bottle neck" in PIC modeling is long time (about 1000 RF periods) for electron quasi-stationary value. To solve this problem the power modulation method was applied at first. It is necessary note that all mentioned above speeding-ups allowed us to reduce PIC simulation time significantly. As a result, one hour computational time on 3 MHz INTEL Pentium processor PC is required to calculate the discharge parameters behavior during 5 μ s of physical time. The computational time was comparable with fluid model (Model 2, see below) simulation time.

The total set of the chemical reactions taken into account in the model is given in Table I.

The well-known cross section set for Ar [8] we tested using MC and two-term approach (TTA) models for electron swarm parameters calculations. The simulation results are in a good agreement with experimental data. It is necessary to note that all excitations in [9] were combined into one total cross section. However plasma chemistry with metastable states and radiation processes could be very important in plasma modeling. For this goal we separated the total cross section from [8] on two parts by the following manner. We used the measured total cross section of metastable states – 3P_2 , 3P_0 taken from [9]. The cascade transactions from upper Rydberg states were taken into account. The total excitation cross section of resonance states was updated by subtraction of the total metastable cross section from the total excitation cross section. The received total resonance states cross section is in a reasonable agreement with calculated the corresponding cross sections for low argon states 3P_1 , 1P_1 with cascade processes taken from [9].

B. Fluid model (Model 2).

1D fluid model of CCP discharge was set up on the base of the commercial multi-physics software package CFD-ACE

[11, 12] (ESI CFD Inc and CFD Research Corp. Huntsville, USA). Detailed formulation of the model and description of the used numerical schemes and solution methods can be found in [12]. The electron transport is described by the electron balance equation, the drift diffusion approximation is used for the electron density flux. The electron temperature T_e is found from the electron energy balance equation. The electron induced reaction rates, the electron mobility and diffusion coefficients as functions of T_e are found by the integration of the corresponding cross sections with the Maxwellian EEDF.

The mass balance equations are solved also for each ion and neutral species. The ion velocities are found from the ion momentum equation. It should be noted that similar to the PIC model the CFD-ACE fluid model takes into account the increase of ion-neutral collisional frequency and thus decrease of the ion mobility in the relatively high electric fields when the ion drift velocity becomes comparable with the thermal velocity of ions. The self-consistent electric field is found by solving the Poisson equation. The voltage at the powered electrode is set as the model input parameter or calculated from the equation of a simple external circuit equation consisting of the power source and one blocking capacitor. Secondary electron emission (SEE) coefficient due to ion flux and kinetic scheme are the same as in model 1.

IV. EXPERIMENTAL AND SIMULATION RESULTS. DISCUSSION.

Figures 2 and 3 show the plasma density measured by a Langmuir probe in the center between the electrodes as a function of the RF power dissipated in the discharge volume at 100 mTorr at 13.56 MHz and 81 MHz respectively. Fig. 4 and 5 show effective RF voltages U_{eff} ($U_{applied} = \sqrt{2} U_{eff}$) applied to the top electrode at 13.56 MHz and at 81 MHz as a function of the RF power. In Fig.6 and Fig.7 plasma density versus U_{eff} at 13.56 MHz and 81 MHz are presented. Figure 8 shows electron temperature versus input power. Curve 1 corresponds to 13.56 MHz, curve 2 – 81 MHz. Values of temperature are received from the analysis of I-V characteristics. Curves were measured by Langmuir probe. It is seen that at the HF frequency excitation both electron density and temperature are higher than at LF.

It is necessary to point out, that in the given experiments the error of electron temperature measurement makes up 0.5 eV. Weak growth of temperature for 81 MHz is observed. The change of temperature in 13.56 MHz is within the limits of measurement accuracy.

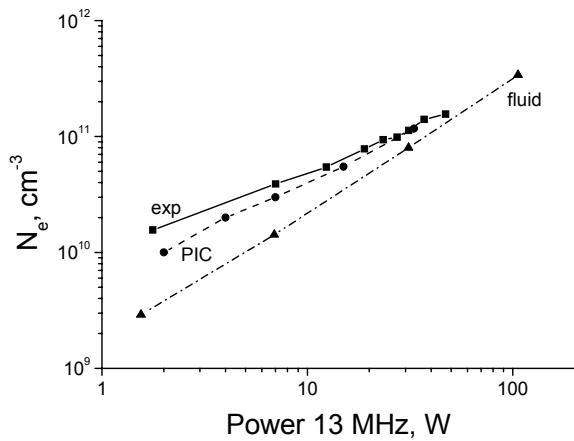


Fig. 2. Electron density in the center of the discharge as a function of the absorbed power, at a frequency of 13.56 MHz. Solid line (exp) – experimental data; dash line (PIC) – results of the PIC model, dot-dash line (fluid) – results of the fluid model.

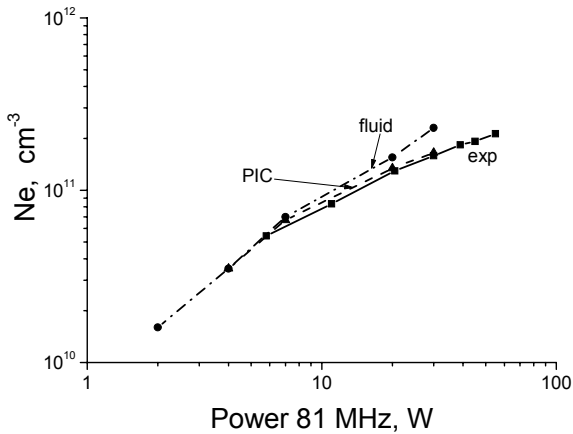


Fig. 3. Electron density in the center of the discharge as a function of the absorbed power, at a frequency of 81 MHz. Notation is the same as in Fig. 2

The simulation at different discharge parameters was carried out to reveal the correlations with experimental data. As it was pointed out in Introduction, to develop adequate model of a DF discharge it is necessary to establish structure and specific features of a Single Frequency (SF) discharge at high input powers. At this stage, experimental observations and measurements, and especially the study of discharge parameters as a function of rf frequency at fixed input powers are of primary importance.

Simulation trends of plasma density against input power and U_{eff} are presented in Fig. 2, 3, 6 and 7 along with experimental data. Calculation values of effective RF voltages U_{eff} are shown in Fig.4 and 5. It is seen that in SF plasma electron density at 81 MHz is essentially higher than at 13.56 MHz at equal power input. The significant decrease of applied voltage with frequency in SF discharge was revealed.

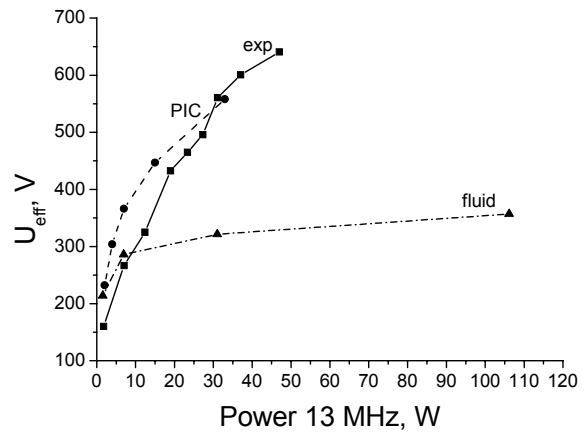


Fig.4. Effective voltage at the powered electrode as a function of the absorbed power, at a frequency of 13.56MHz. Notation is the same as in Fig.2

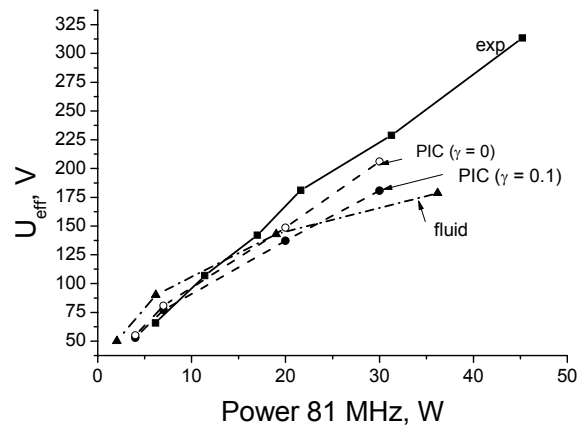


Fig.5. Effective voltage at the powered electrode as a function of the absorbed power, at a frequency of 81 MHz. Notation is the same as in Fig. 2. PIC simulation: full circle – $\gamma=0.1$; open circle – $\gamma=0$.

The simulation results of Model 1 at LF frequency are in a reasonable accordance with experimental data (Fig.2,4,6). Note that the discharge at 13.56 MHz is operated gamma-mode in all range of experimental values of input powers [13-15]. According to [13] the transition from alfa to gamma mode at this RF frequency is observed at $U_{eff} \approx 60-75$ V at Ar pressure of 100 mTorr. This voltage value is lower than our experimental voltages. Electron cathode beam produced by secondary electron emission (SEE) from the electrode due to the ion bombardment starts to be significant ionization source. A reasonable for Ar ions value $\gamma=0.1$ was used in simulation. In this case, PIC MC model (Model 1) quite adequately describes the experimental results.

It is necessary to note that at these LF and Ar pressure range α - γ mode transition has weakly pronounced hysteresis structure in volt-current dependence without sharp current increasing after the discharge reconstruction to γ mode operation [13]. At these plasma conditions, the ionization length of the secondary electrons exceeds the sheath width. As a result, the ionization events will take place not only near

sheath boundary but also in the quasi-neutral plasma region. So there is no sheath breakdown at these plasma conditions. It was shown [13] that the plasma impedance is capacitive in such conditions.

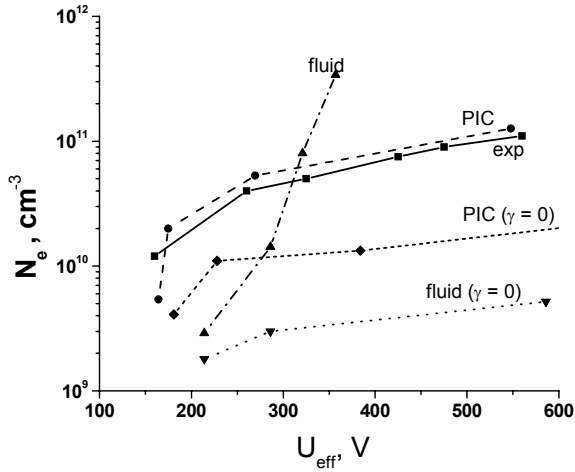


Fig.6. Electron density in the center of the discharge as a function of the effective voltage at the powered electrode, at a frequency of 13.56 MHz. Solid line (exp) – experimental data; dash line (PIC) – results of the PIC model, dot-dash line (fluid) – results of the fluid model; shot-dash line (PIC ($\gamma=0$)) – results of the PIC model without secondary electron emission; dot line (fluid ($\gamma=0$)) – results of the fluid model without secondary electron emission.

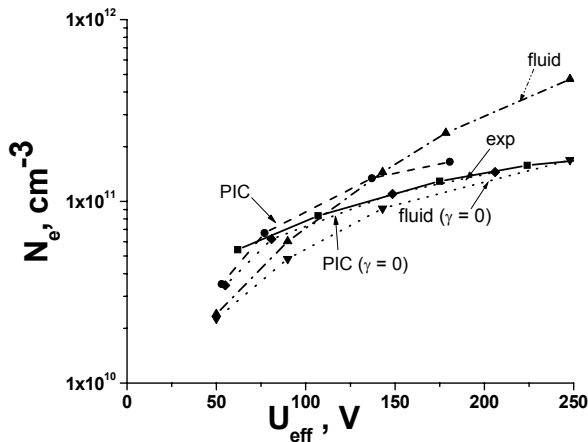


Fig.7. Electron density in the center of the discharge as a function of the effective voltage at the powered electrode, at a frequency of 81 MHz. Notation is the same as in Fig. 6

As an example, calculated time dependences of the discharge current and voltage at 33 W powers are presented in Fig. 9a. The similar results are observed for others input powers. As it seen the total current and voltage are near $\pi/2$ radian out of phase. The total current through the discharge is established by the displacement current in the sheaths because of small parts of the electron and ion currents (Fig. 9b). It corresponds to capacitive plasma impedance.

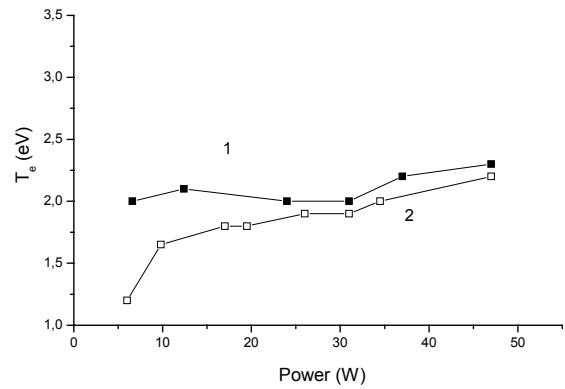


Fig. 8. Experimental electron temperature versus power. 1 – 13.56 MHz; 2 – 81 MHz.

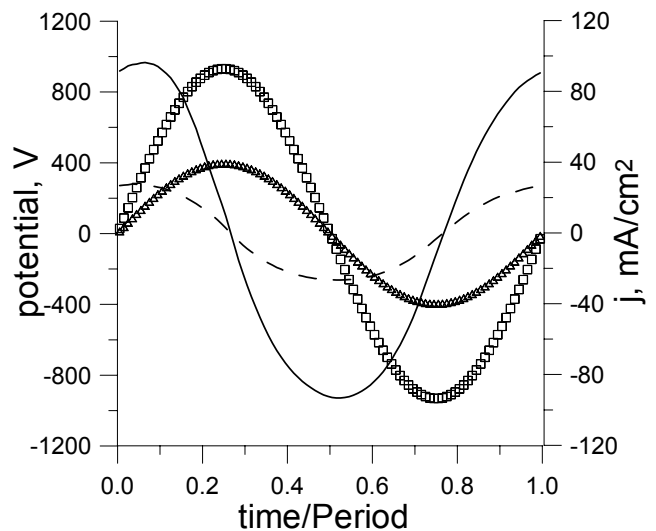


Fig. 9a. Time dependence of the discharge current and the voltage at the powered electrode at a frequency of 13.56 MHz and at different input powers (PIC model). Line – current (solid line – 33 W, dash line – 3 W), symbols – voltage (squares – 33 W, triangles – 3 W).

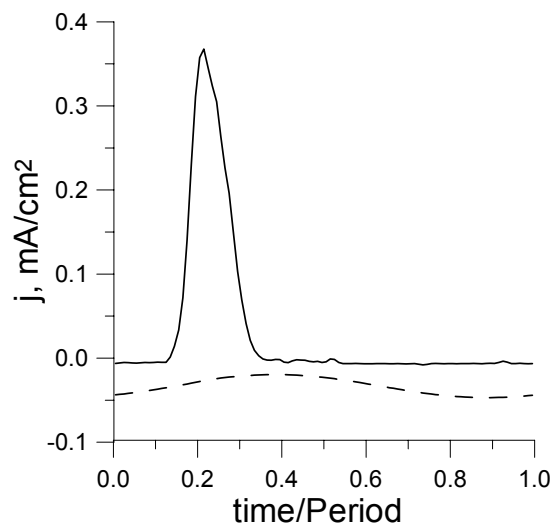


Fig. 9b. Time dependence of the electron and ion currents at the powered electrode at a frequency of 13.56 MHz and an input power of 33 W (PIC model).

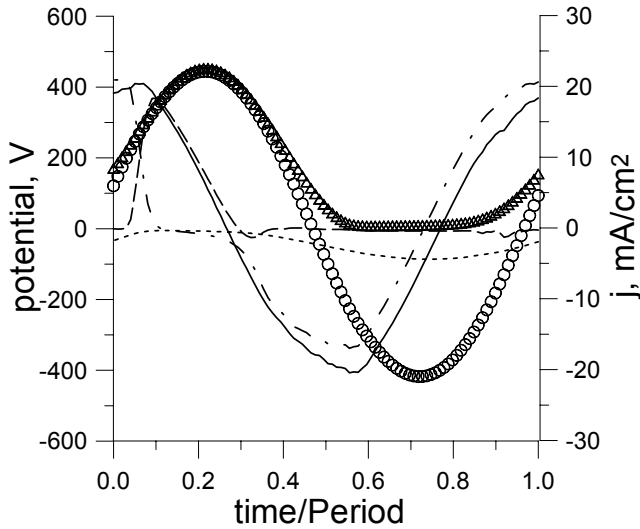


Figure 9c. Time dependence of the total discharge current (solid line), electron current (dash line), ion current (shot-dash line), displacement current (dot-dash line) and the voltage (circle symbols) at the powered electrode at a frequency of 13.56 MHz and an input power of 100W (fluid model). Triangle symbols – plasma potential in the center of the discharge.

It should be emphasized once more that the comparison of discharge parameters at different frequencies should be carried out at the same fixed power rather than applied voltage. So, for example, it was concluded in [4] that plasma potential of a SF discharge is weakly dependent on frequency. Such conclusion was done based on discharge simulation under fixed discharge voltage. However, as it seen from Fig. 4 and 5 at the same voltage, for example 150 V, input power at 80 MHz is in ~10 times higher than input power at 13.56 MHz! Simulation results using Model 2 with $\gamma=0.1$ are presented in Fig. 2, 4 and 6 for LF discharge. As it seen from Fig.2, simulation results are lower than experimental plot. As appears from Fig. 4, values U_{eff} in Model 2 are substantially lower than in Model 1 for the same power inputs. Moreover, sharp turn is observed on U_{eff} dependence of plasma density (Fig. 6). Such character of α - γ mode transition is typical for high pressures ($p > 1$ Torr) [13] and corresponds to sheath breakdown. Non-sinusoidal behavior of discharge current provides additional confirmation of this statement. Similar dependences are described in [16] for helium like plasma and in [17] in helium plasma at pressure of 3 Torr and $\gamma=0.2$. As an example, calculated temporal dependences of the discharge current at 100 W power ($U_{eff}=320$ V) using Model 2 are presented in Fig. 9c. The triangular shape of discharge current indicates on strong non-linear discharge impedance and a more resistive sheath. Thus, the transition to γ -mode in Model 2 takes place at $U_{eff} \sim 280$ V. The structure of this transition is similar to the collisional ones. It connects with not correct simulation of SEE in Model 2.

Calculated results for Models 1 and 2 with $\gamma=0$ are also presented in Fig. 6, indicating important role of both beam electrons and non-local features of bulk electrons. To illustrate the important role of both SEE and non-local effects in electron heating at the studied conditions the spatial

distributions of electron input power at 3 W total power and ionization rate for both 3 W and 33 W total powers calculated in Model 1 at 13.56 MHz are shown in Fig. 10a and 10b respectively. Data for 33 W were presented both with SEE and without SEE taking into account. In Fig. 11 Electron Energy Distribution Functions (EEDF) in the centre of discharge are presented for different input powers.

As it is seen from Fig. 10a, the main electron power deposition is realized in the sheaths even at power 3 W. But the spatial distribution of the ionization rate has a flat profile due to non-local nature of discharge (Fig. 10b). Simulation result with $\gamma=0$ for power 33 W is shown in Fig. 10b also. It is seen that the spatial distribution of the ionization rate without SEE is peaked in the bulk of discharge. The profiles of EEDF in Fig. 11 indicate that at high power (33 W) the “tail” of fast electrons (energies greater than 25-30 eV) is greater than at 3 W rf power. The exclusion of γ electrons from simulation results in significant decreasing of the fast electron tail and EEDF increasing near ionization potential energies ~12-30 eV. It results in the plasma density decrease and electric field increase, and as a result in mean electron energy increase.

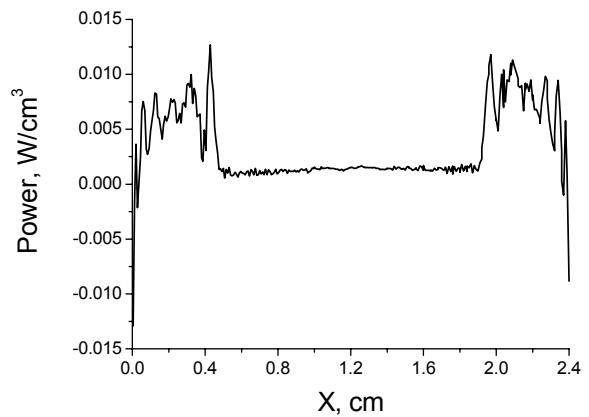


Figure 10a. Spatial distribution of the power density absorbed by electrons at a frequency of 13.56 MHz and an input power of 3W (PIC model).

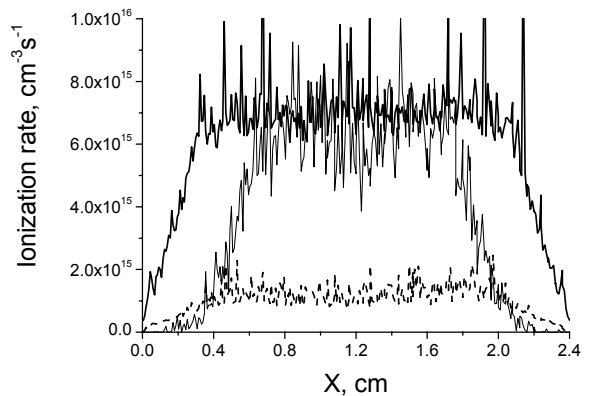


Figure 10b. Spatial distribution of the ionization rate at a frequency of 13.56 MHz at different input powers (PIC model). Thick solid line – 33W, dash line – 3W, thin solid line – 33W without secondary electron emission ($\gamma=0$).

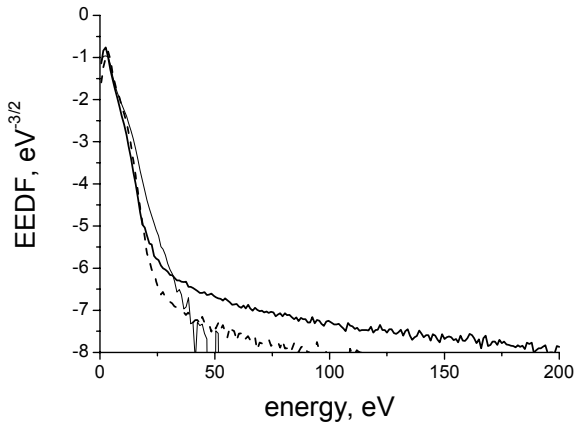


Figure 11. Electron energy distribution function (EEDF) in the center of the discharge at a frequency of 13.56 MHz at different input powers (PIC model). Thick solid line –33W, dash line – 3W, thin solid line – 33W without secondary electron emission ($\gamma=0$).

Consider the specific features of HF (81 MHz) discharges in the same range of input powers. Calculated and experimental results are presented in Fig. 3, 5 and 7. As it followed from Model 1, the HF discharge is in α -mode for entire range of input powers. To illustrate the fact that the HF discharge is burnt in near α -mode for all input powers, i.e. SEE is not so significant for HF discharge, the plasma density calculated by Models 1 and 2 with $\gamma=0$ are shown in Fig. 7. Calculations of electron density for Model 2 ($\gamma = 0$) as a function of input power and voltage are in good agreement with Model 1 ($\gamma = 0$). The small difference shows that description of non-local behavior of bulk electrons using electron energy equation is quite adequate for these HF discharges.

It is necessary to note that small differences between experimental and calculated results could be connected with plasma burning not only in electrode gap but outside electrode region especially at high input powers. In this case non one-dimensional feature of the discharge is revealed for both frequencies. Thus, to compare calculated and experimental data we used effective electrode area of 10 cm in diameter rather than $D_{\text{electrode}}=8$ cm.

It should emphasize also one important moment. In simulation of both LF and HF discharges at high power inputs, it should control also the applicability of different approaches for ion kinetics. As it was noted above, ion inertia is taken into account using ion momentum equation. However, for high powers, it is necessary to take into account non-constant behavior of ion mobility in strong sheath fields. Accurate description of this effect is possible in kinetic approaches for ions. Standard ion mobility μ should be corrected when ion drift velocity is comparable with ion thermal velocity v_T [18]. Effectively it means that in general case ion mobility μ_{eff} could be approximated as follows.

$$\mu_{\text{eff}} = \frac{\mu}{1 + \sqrt{\mu|E|/v_T}} \quad (16)$$

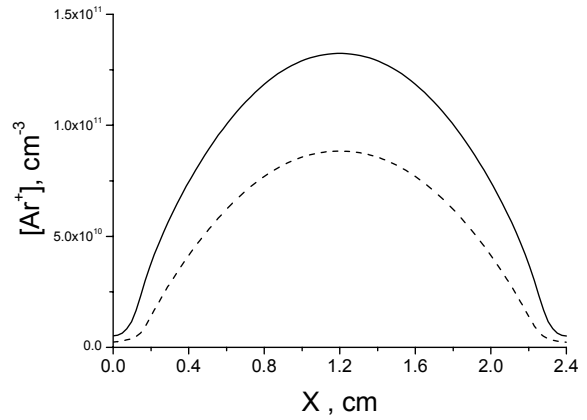


Fig.12. Spatial distribution of the ion Ar^+ density at a frequency of 81MHz and an effective voltage at the power electrode $U_{\text{eff}}=140$ V. Solid line – results of the fluid model with ion mobility correction (see the text), dash line – results of the fluid model without ion mobility correction

The use of this approach in our case is grounded on collision mode for ions in both LF and HF discharges. Our experiments show that kinetic approach for ions is required for pressures lower than 45 mTorr. As an illustration, Fig. 12 shows calculated (Model 2) distributions of plasma density with and without ion mobility correction (16). As it seen, plasma density profile is changed substantially if mobility correction is not taken into account.

Note that gas temperature was not measured experimentally. The results of simulation show that spatial distribution of T_g has a typical Bessel profile. Maximal values of T_g in the center of discharge at high powers are not exceeded 440 K for HF (30 W) and 337 K for LF (33W).

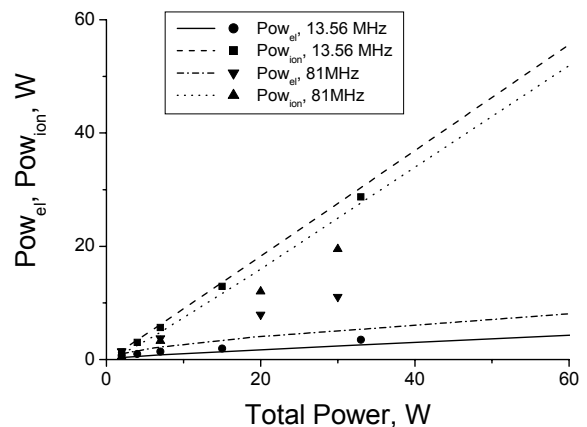


Fig.13. Power absorbed by electrons (P_{el}) and by ions (P_{ion}) as functions of the total input power. Lines – results of the fluid model, symbols – results of the PIC model.

Fig. 13 shows calculated (Model 1 and 2) averaged over period and gap powers absorbed by electrons P_{el} and ion P_{ion}

as functions of total input power P_{input}

$$P_{input} = P_{el} + P_{ion} = \int (j_{el} E) dxdt + \int (j_{ion} E) dxdt \quad (17)$$

for 13.56 MHz and 81 MHz, respectively. As it seen from this figure, that description of electron and ion absorbed power redistribution at different total input powers is close for both models. Nevertheless, as it seen from Fig. 13, for discharge at HF, more correct kinetic approach for electrons (Model 1) increases energy absorbed by electrons in comparison with Model 2.

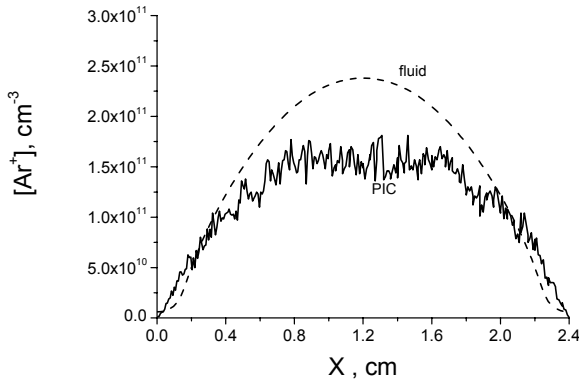


Fig.14a. Spatial distribution of the ion Ar^+ density at a frequency of 81MHz. Solid line – results of the PIC model at an input power of 30W, dash line – results of the fluid model at an input power of 36W.

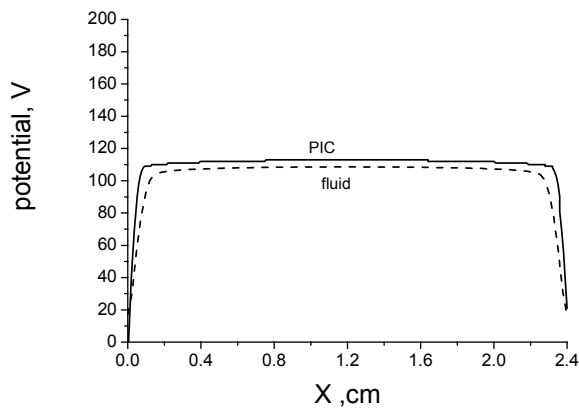


Fig.14b. Spatial distribution of the electric potential at a frequency of 81MHz. Solid line – results of the PIC model at an input power of 30W, dash line – results of the fluid model at an input power of 36W

As it followed from our study and analysis of different approaches to simulation of LF and HF discharges at high specific input powers, more simple fluid model with ion mobility correction could be used for optimization of technological processes and prediction of plasma densities as functions of input powers. The possibility to have such dependences and trends on the base of fast model allows to carry out express analysis of the reactor processes in complex gas mixtures used in the technology.

However, it should understand that for detail study of

discharge structure kinetic approach for electrons and, in some conditions, for ions is necessary. As an illustration, Fig. 14-16

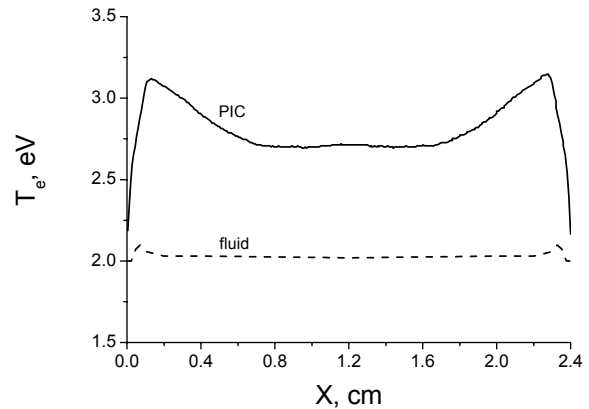


Fig.15. Spatial distribution of the averaged electron temperature at a frequency of 81 MHz. Solid line – results of the PIC model at an input power of 30W, dash line – results of the fluid model at an input power of 36W

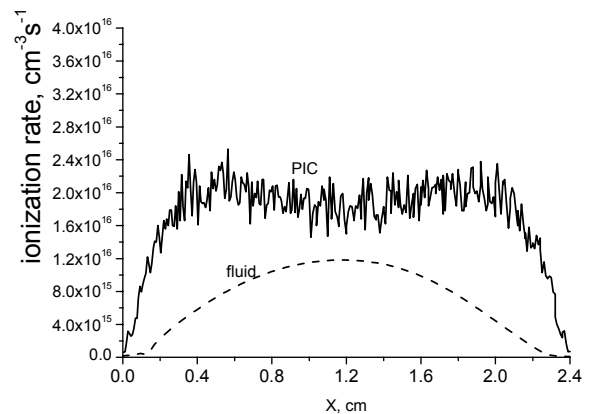


Fig.16. Spatial distribution of the ionization rate at a frequency of 81MHz. Solid line – results of the PIC model at an input power of 30W, dash line – results of the fluid model at an input power of 36W

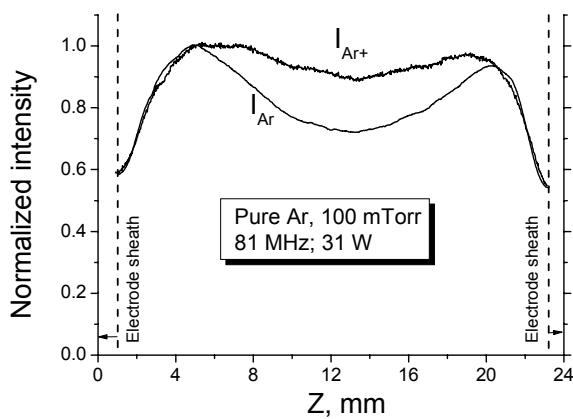


Fig. 17. Typical spatial distribution of Ar($2p_1-1s_2$ transition - 750 nm) and Ar⁺(470 nm) emission in the interelectrode gap of the 81 MHz CCP discharge at pressure of 100 mTorr (RF power 31 W). “0 mm” is a position of the powered electrode, “24 mm” is a position of the grounded electrode. Vertical dashed lines show approximate positions of the electrode sheaths.

show spatial distributions of averaged over period plasma density, electric field potential, electron temperature and ionization rate returned by Model 1 and 2. Fig. 15 and 16 show, that kinetic approach for electrons in weakly collisional α -mode results in electron temperature and ionization rate increase in pre-sheaths because of non-local behavior of electron energy spectrum. This fact is confirmed by our optical emission measurements. Fig 17 shows the experimental data on spatial distribution of atomic and ion argon lines for the conditions of Fig.16. The comparison of Fig. 16 and 17 shows that kinetic approach for electrons is required for correct description of discharge spatial structure.

V. CONCLUSION

The CCP discharges in Ar in single (LF of HF) frequency mode at pressure 100 mTorr and high specific input powers have been investigated both theoretically and experimentally. The Lagnmuir probe was used for measuring the plasma density. The spectrograph and imaging ICCD system were used for characterizing the spatial structure of electronic excitations in the discharge.

Different kinetic and fluid models were developed and used. It was shown:

- The 13.56 MHz discharges are burnt in γ mode for applied voltages and input powers under study.
- There is a good agreement of experimental and simulated (Model 1 with secondary electron-ion emission coefficient $\gamma=0.1$) dependences for LF discharge.
- 81 MHz discharges are burnt in α -mode for applied voltages and input powers under study.
- There is a reasonable agreement between experimental and simulated dependences of plasma density as a function input power and applied voltage for 81 MHz discharges.
- Ion mobility correction is necessary to take into account

in strong sheaths fields.

- Kinetic approach for electrons is required for correct description of discharge spatial structure.

REFERENCES

- [1] H.C. Kim and V.I. Manousiouthakis, *J. Vac. Sci. Technol.* A16, p.2162, 1998
- [2] V.Vahedi and G.DiPeso, *J. Comput. Phys.*, vol.131, p.149, 1997
- [3] V.Georgieva, A.Bogaerts and R.Gijbels, *J. Appl. Phys.*, vol.94, pp.3748-3756, 2003
- [4] J.K. Lee, N.Yu. Babaeva, H.C. Kim, O.V.Manuilenko and J.W. Shon, *IEEE Trans. Plasma Sci.*, vol.32, pp.47-53, 2004
- [5] V. Ivanov, O. Proshina, T. Rakhimova, A. Rakhimov, D. Herrebut and A. Bogaerts, *J. Appl. Phys.*, vol.91, pp.6296-6302, 2002.
- [6] V.V.Ivanov, A.M.Popov, T.V.Rakhimova, *Plasma Phys. Rep.*, v.21, p.515, 1995
- [7] A.V.Phelps, *J.Phys. Chem. Ref. Data*, vol.20, pp. 557-573 (1990)
- [8] A.V.Phelps, *JILA Information Center Report*, N28, 1985
- [9] N.J. Mason and W.R. Newell, *J.Phys. B; At. Mol. Phys.*, vol. 20, pp.1357-1377, 1987
- [10] H.A. Hyman, *Phys. Rev. A20*, pp.855-859, 1979
- [11] http://www.esigroup.com/SimulationSoftware/CFD_ACE/appl_plasma.html and <http://www.cfdrc.com/~cfdplasma/>.
- [12] *CFD-ACE+ User Manual, Plasma Module Manual*, Copyright © 1994-2005 ESI Group.
- [13] V.A. Lisovski, *Technical Physics*, vol.43, p.526, 1998
- [14] Yu.P. Raizer, M.N. Shneyder and N.A. Yatsenko, *Radiofrequency capacitive coupled discharge*, Moscow, Nauka, 1995.
- [15] M.A. Liberman and A.J.Lichtenberg, *Principle of Plasma Discharges and Material Processing*, New York, Wiley,1994.
- [16] M.Surendra and D.B.Graves, *IEEE Trans.Plasma Science*, vol.19, p.144, 1991.
- [17] Ph.Belenguer and J.P. Boeuf, *Phys.Rev. A*, vol.41, p.4447, 1989.
- [18] Yu.P. Raizer, *Gas Discharge Physics*, Springer-Verlag, Berlin, 1991.